Journal of Micromechanics and Molecular Physics
Vol. 3, Nos. 3 & 4 (2018) 1840009 (31 pages)

DOI: 10.1142/S242491301840009X

World Scientific
www.worldscientific.com

Cosserat crystal plasticity with dislocation-driven grain boundary migration

Anna Ask*, Samuel Forest*,‡, Benoit Appolaire† and Kais Ammar*

*MINES ParisTech, PSL Research University
MAT – Centre des Matériaux, CNRS UMR 7633
BP 8791003 Evry, France

†Institut Jean Lamour, Université de Lorraine
2 Allée André Guinier 54000 Nancy, France
‡samuel.forest@ensmp.fr

Received 27 July 2018
Revised 6 October 2018
Accepted 11 October 2018
Published 17 December 2018

Abstract This paper discusses a coupled mechanics–phase-field model that can predict microstructure evolution in metallic polycrystals and in particular evolution of lattice orientation due to either deformation or grain boundary migration. The modeling framework relies on the link between lattice curvature and geometrically necessary dislocations and connects a micropolar or Cosserat theory with an orientation phase-field model. Some focus is placed on the underlying theory and in particular the theory of dislocations within a continuum single crystal plasticity setting. The model is finally applied to the triple junction problem for which there is an analytic solution if the grain boundary energies are known. The attention is drawn on the evolution of skew–symmetric stresses inside the grain boundary during migration.

Keywords Crystal plasticity; Cosserat; non-local theory; phase-field method; dislocation density tensor.

1. Introduction

By controlled thermomechanical processing, the microstructure of metallic polycrystals can be manipulated in order to obtain certain desired material properties. A typical example is cold working followed by annealing, where energy is stored in the material during viscoplastic deformation and later released by nucleation and growth of new grains during a process known as static recrystallization. Deformation at elevated temperatures on the other hand may lead to concurrent (dynamic) recrystallization [Humphreys and Hatherly, 2004].

Simulation models for microstructure evolution in metals can be formulated at length scales from the atomistic up to the continuum level. Models at the lower

‡Corresponding author.

scales (atomistic simulations, molecular dynamics) are computationally demanding due to their very high resolution and not feasible for polycrystals undergoing load sequences which may last minutes or hours. On the other hand, a macroscopic model which retains no information about the microstructure is too coarse. The most promising models are therefore formulated at the mesoscopic level, resolving the grain structure but not individual atoms, defects or dislocations.

Several authors have developed modeling approaches for recrystallization processes which rely on coupling continuum single crystal plasticity with methods for nucleation and/or grain boundary motion. For the nucleation, probabilistic methods or methods based on some selection criteria (such as stored energy or lattice curvature) are often adopted. There exist a number of methods to deal with migrating grain boundaries such as probabilistic cellular automata (CA) and Monte-Carlo-Potts models, vertex models, phase-field and level-set models [Rollett, 1997; Humphreys and Hatherly, 2004; Gottstein and Shvindlerman, 2010; Hallberg, 2011]. Out of these, phase-field and level-set models that do not explicitly track the moving fronts are the most well-suited for strongly coupled approaches as they result in systems of partial differential equations which can in practice be solved by the same methods as the crystal plasticity equations. The level-set approach has been used by Bernacki *et al.* [2009] for primary recrystallization in polycrystalline materials based on the finite element method. On the other hand, it is straightforward to incorporate phase-field models in the thermodynamic framework of continuum mechanics using the concept of generalized stresses by Gurtin [1996], Gurtin and Lusk [1999] and Ammar *et al.* [2009a]. This approach has been explored by e.g., Ammar *et al.* [2009b, 2011], de Rancourt *et al.* [2016], Hektor *et al.* [2016] to model diffusion-controlled phase transformations in elastoplastic media.

To model static recrystallization, the most common approach in the literature is to couple a crystal plasticity modeling step with subsequent nucleation and grain migration steps. For example, a strain gradient crystal plasticity finite element approach was used by Takaki *et al.* [2007, 2009] to compute the crystal orientations and dislocation densities in a deformed polycrystal. The results were then mapped onto another discretized grid and the microstructure was evolved using a phase-field approach. Nucleation sites were identified based on criteria of misorientation and stored energy. A similar approach was explored by Güvenç *et al.* [2013, 2014]. A dislocation-based crystal plasticity finite element approach was followed by a nucleation step using the calculated dislocation densities as an input variable. The evolution of the microstructure was then modeled using a phase-field model in a finite different scheme. Vondrous *et al.* [2015] combined a standard crystal plasticity finite element model with a phase-field step solved by finite differences to simulate static recrystallization in large samples and three dimensions. Another approach for sequential recrystallization was presented by Chen *et al.* [2015] who used a spectral fast Fourier transform (FFT)-based solver for both the crystal plasticity and the phase-field equations. The treatment of the crystal plasticity was restricted

to small deformations and nucleation sites were predicted based on accumulated plastic strain. Similar to the previous works mentioned, the crystal plasticity calculations preceded the phase-field calculations, although a staggered scheme was then applied so that the mechanical equilibrium was ensured after each phase-field time step. Abrivard *et al.* [2012a,b] adopted the formalism of Gurtin and Lusk [1999] and Ammar *et al.* [2009a] and solved the single crystal plasticity and phase-field equations by finite elements. The crystal orientations and stored energies were calculated in the deformation step and then used as input in the phase-field simulations to find the new microstructure.

Similar coupled approaches have been adopted for dynamic recrystallization. Takaki *et al.* [2014] coupled an elasto-plastic finite element model with a phase-field model solved by finite differences in a type of staggered scheme whereas Zhao *et al.* [2016] coupled FFT-based crystal plasticity simulations with a statistical nucleation model and phase-field simulations. Blesgen [2017] coupled a non-local Cosserat crystal plasticity model with a recovery and nucleation step and grain boundary migration modeled by the level-set method in a staggered scheme.

While the sequentially or weakly coupled approaches listed above are able to capture important features of the recrystallization process, they do not represent a unified, thermodynamically consistent theory of microstructure evolution in polycrystals. Recently, Ask *et al.* [2018b] and Admal *et al.* [2018] have proposed such strongly coupled models based on higher-order single crystal plasticity theories and an orientation phase-field method originally introduced by Kobayashi *et al.* [2000], Warren *et al.* [2003]. Orientation phase-field models are well suited for coupling with crystal plasticity models as they rely on a continuous representation of lattice orientation both at grain boundaries and inside the grains. This is in contrast to methods that rely on a cellular description of the microstructure with constant orientation within each cell or grain, such as Monte-Carlo-Potts models, CA or vertex models.

The coupled crystal plasticity-phase-field approach proposed by Admal *et al.* [2018] relies on a strain gradient plasticity approach in the spirit of [Cermelli and Gurtin, 2001; Gurtin, 2002]. A non-standard free energy function based on a phase-field order parameter and the tensor of so-called geometrically necessary dislocations (GND) is formulated, inspired by the orientation phase-field model of Kobayashi *et al.* [2000] and Warren *et al.* [2003]. This results in a model capable of predicting grain boundary migration on the one hand due to capillary forces (grain boundary curvature) and on the other hand due to shear-induced grain boundary motion and grain sliding. The formulation relies on introducing the plastic slips on each slip system as kinematic variables with their own associated microstress balances and the representation of grain boundaries in terms of GND. Grain boundary motion in the model by Admal *et al.* [2018] is accommodated by plastic slip processes.

In the present work, a coupled crystal plasticity-phase-field model introduced by Ask *et al.* [2018b] is revisited. In order to take into account non-local effects, a

Cosserat or micropolar [Cosserat and Cosserat, 1909; Eringen and Kafadar, 1976; Forest *et al.*, 1997] approach is adopted and the lattice orientation changes of the crystal are associated on the constitutive level with the Cosserat microrotations, which enter as additional degrees of freedom. It was shown in Ask *et al.* [2018b] that such a modeling approach allows evolution of lattice orientation at a material point, both due to viscoplastic deformation and grain boundary migration. The considered driving forces for grain boundary migration were capillary forces as well as stored energy due to scalar dislocation densities accumulated during deformation. The model allows for reorientation of the crystal lattice due to plastic slip processes but grain boundary migration mechanism is not associated directly with plastic slip. A linearized version of the model by Ask *et al.* [2018a] is used in this work and applied to the solution of the triple junction problem, where three grains meet at a common point. The objective is to study the development and relaxation of skew–symmetric stresses predicted by the model in the moving grain boundaries and at the triple junction.

This article is structured as follows. The first two sections discuss important aspects of the phase-field method and crystal plasticity theory, respectively. The third section presents the coupled Cosserat crystal plasticity phase-field framework. This is followed by a section dedicated to the numerical solution to the triple junction problem. The paper is concluded with a summary of the presented theory and the outlook for future work.

Notation

Vectors and second-order tensors are denoted by $\underline{\boldsymbol{a}}$ and $\underset{\sim}{\boldsymbol{A}}$, with the transpose $\underset{\sim}{\boldsymbol{A}}^T$. Third-order tensors are given by $\underline{\underline{\boldsymbol{a}}}$ and fourth-order tensors by $\underset{\approx}{\boldsymbol{C}}$. In particular, $\underset{\sim}{\boldsymbol{I}}$ is the second order identity tensor and $\underline{\underline{\boldsymbol{\epsilon}}}$ is the third-order Levi-Civita permutation tensor. The latter is used to express skew-symmetric tensors as pseudo-vectors

$$\overset{\times}{\underline{\boldsymbol{A}}} = -\frac{1}{2}\underline{\underline{\boldsymbol{\epsilon}}} : \operatorname{skew}(\underset{\sim}{\boldsymbol{A}}) = -\frac{1}{2}\underline{\underline{\boldsymbol{\epsilon}}} : \underset{\sim}{\boldsymbol{A}}, \tag{1.1}$$

and vice versa

$$\operatorname{skew}(\underset{\sim}{\boldsymbol{A}}) = -\underline{\underline{\boldsymbol{\epsilon}}} \cdot \overset{\times}{\underline{\boldsymbol{A}}}. \tag{1.2}$$

Double contraction is denoted $\underset{\sim}{\boldsymbol{A}} : \underset{\sim}{\boldsymbol{B}}$ and simple contraction is written as $\underline{\boldsymbol{b}} = \underset{\sim}{\boldsymbol{A}} \cdot \underline{\boldsymbol{a}}$. The scalar product of two vectors is $\underline{\boldsymbol{a}} \cdot \underline{\boldsymbol{b}} = \underline{\boldsymbol{a}}^T \underline{\boldsymbol{b}}$. On the other hand, $\underset{\sim}{\boldsymbol{A}} = \underset{\sim}{\boldsymbol{a}} \otimes \underset{\sim}{\boldsymbol{b}}$ indicates the dyadic or tensor product of two vectors. The gradient of a vector is written as $\underline{\boldsymbol{a}} \otimes \nabla$ and the divergence of a vector or tensor is written as $\nabla \cdot \underline{\boldsymbol{a}}$ or $\underset{\sim}{\boldsymbol{A}} \cdot \nabla$, respectively (differentiation of a tensor is assumed to act on the second index). The curl operator is denoted $\nabla \times \underset{\sim}{\boldsymbol{A}}$. In case, a distinction is made between the deformed and reference configurations, differentiation with respect to the reference coordinates is denoted by ∇_0.

2. Phase-Field Approaches for Grain Boundary Migration

There exist several mathematical approaches that deal with the dynamics of moving interfaces. One such approach is the phase-field method. A phase-field model of Allen–Cahn type [Allen and Cahn, 1979] considers a non-conserved order parameter ϕ (the phase-field) which takes distinct values for each phase in the bulk and varies fast but continuously over interface regions. The free energy of the system associated with the phase-field is given by

$$\mathcal{F}_{\mathrm{PF}} = \int_{\Omega} \psi_{\mathrm{PF}}(\phi, \nabla\phi)\mathrm{d}\Omega = \int_{\Omega} \left[f(\phi) + \frac{a^2}{2}|\nabla\phi| \right] \mathrm{d}\Omega. \tag{2.1}$$

It is then postulated that the dynamics of the phase-field can be found from the (vanishing) variational derivative of $\mathcal{F}_{\mathrm{PF}}$ according to

$$\eta_\phi \dot{\phi} = -\frac{\delta\mathcal{F}}{\delta\phi}, \tag{2.2}$$

where η_ϕ is a viscosity type parameter that controls the timescale of relaxation towards equilibrium and thereby the mobility of the interface. The contribution $f(\phi)$ to the energy density essentially determines the composition of different phases in the bulk. For two separate phases, such as liquid or solid, $f(\phi)$ is, in general, a double-well polynomial with one local minima for each of the two corresponding values of ϕ. The gradient term $\frac{a^2}{2}|\nabla\phi|$ represents the interface energy and localizes the grain boundaries to regions of width proportional to the parameter a.

In a solid polycrystal of a single phase material, grains are distinguished by their relative lattice orientations. The above standard model is not directly applicable to the problem of grain boundary migration in this case. Instead, extended approaches based on the general idea of the generic phase-field model have been proposed. In the so-called MPF method, the orientations are represented indirectly by assigning each orientation or grain an order parameter, whereas in the orientation phase-field approach, the crystal orientation itself is considered an order parameter. A brief outline of both methods will be given below. The discussion will focus on grain boundary migration in solid polycrystals, although both models have a wider scope of possible applications.

2.1. *MPF model*

Adopting the multiphase-field MPF approach [Steinbach *et al.*, 1996; Steinbach and Pezzolla, 1999], each crystal or rather crystal orientation can be represented by one of in total N non-conserved phase-field variables ϕ_i, $i = 1, \ldots, N$. The ϕ_i are not independent as the sum of all fields at any one point is one, i.e., $\sum_i^N \phi_i = 1$. Each phase-field furthermore takes the value one for a unique grain or orientation and is zero in all other grains. Several phases at once are present only at interfaces (two fields at a boundary between two grains, three fields at a triple junction and so on). The phase fields are not themselves the orientation but rather represent

the volume fraction of phase i, corresponding to a given orientation, present at a material point. The following equations govern a multiphase-field problem with N individual phases [Steinbach, 2009]. First, the energy is given by

$$\mathcal{F}_{\mathrm{MPF}} = \int_{\Omega} \sum_{i=1}^{N} \frac{4\sigma_{ij}}{a} \left[-\frac{a^2}{\pi} \nabla\phi_i \cdot \nabla\phi_j + \phi_i \, \phi_j \right] \mathrm{d}\Omega. \tag{2.3}$$

Note that for $N = 2$ and $\phi_j = 1 - \phi_i$, the term $\phi_i \, \phi_j$ represents a double obstacle potential rather than a double well [Steinbach and Pezzolla, 1999]. The parameters σ_{ij} and a represent the interface energy between the phases and the interface width, respectively. Second, the evolution of the phase-field ϕ_i can be found from

$$\dot{\phi}_i = -\sum_{j=1}^{N} \frac{\pi^2}{8aN} M_{ij} \left[\frac{\delta\mathcal{F}_{\mathrm{MPF}}}{\delta\phi_i} - \frac{\delta\mathcal{F}_{\mathrm{MPF}}}{\delta\phi_j} \right], \tag{2.4}$$

where M_{ij} is the mobility of the interface.

It is possible to account for a large number N of phase fields and thus individual orientations, but the MPF approach still has limitations when it comes to representing a real microstructure. In particular, this is the case when viscoplastic deformations are taken into account as these may lead to considerable microstructural changes including heterogeneous lattice orientation developing even within grains. In the MPF model, the grains are considered as having homogeneous orientation and reinitializing the grain structure would be necessary to take into account the formation of new subgrains due to deformation. It is not evident how a strongly coupled theory would deal with updating the orientation at individual material points due to concurrent viscoplastic deformation and grain boundary migration. The MPF model has nevertheless been successful in sequentially coupled approaches [Takaki *et al.*, 2009; Takaki and Tomita, 2010; Güvenç *et al.*, 2013, 2014; Vondrous *et al.*, 2015] to model static or dynamic recrystallization.

2.2. *Orientation phase-field model*

In the model by Kobayashi *et al.* [2000] and Warren *et al.* [2003] (which will be referred to hereafter as the KWC model), the basic phase-field model is extended by considering also the crystal orientation to behave as a phase-field, varying continuously over interfaces between grains and having its own relaxational dynamics. It is clear that this approach differs considerably from the MPF model. First, only two fields are necessary to represent the crystal structure. For a pure solid, the field $\phi \in [0, 1]$ is considered a coarse-grained order parameter which takes the value, one in a perfect crystal and goes to zero in the grain boundaries. The KWC model was formulated in two dimensions, allowing the crystal orientation everywhere to be represented by the scalar field θ representing a rotation around the out-of-plane axis relative to a fixed frame. Second, this representation of the crystal orientation as a continuous field allows for heterogeneities to develop even inside grains. This makes

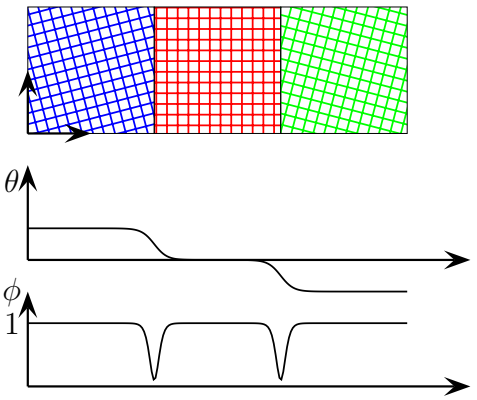

Fig. 1. Schematic representation of the profiles of the orientation θ and order parameter ϕ phase fields in the KWC model for a single-phase solid polycrystal.

the KWC approach particularly well suited to couple with a viscoplastic continuum mechanics theory. A schematic representation of the profiles of the phase-fields in the KWC model is shown in Fig. 1 for a single-phase solid.

As the orientation is measured relative to some fixed frame, only its gradient enters the energy density. Kobayashi *et al.* [2000] showed that two terms are necessary to include: a linear term in $|\boldsymbol{\nabla}\theta|$ in order to energetically favor localized grain boundaries, and (at least) a higher-order term $|\boldsymbol{\nabla}\theta|^2$ to smooth the profiles of η and θ to allow for the grain boundaries to be mobile. For small misorientations, $\nabla\theta$ is a measure of the lattice curvature. Later, in this paper, the relation between lattice curvature and dislocations will be elaborated and the connection to higher-order crystal plasticity theories will be discussed.

The specific dimensionless (overbar indicates non-dimensionalized operators and parameters) KWC energy takes the form

$$\overline{\mathcal{F}}_{\mathrm{KWC}} = \int_{\overline{\Omega}} \left[f(\phi) + \frac{\overline{a}^2}{2} |\overline{\nabla}\phi|^2 + \overline{s} g(\phi) |\overline{\nabla}\theta| + \frac{\overline{\varepsilon}^2}{2} h(\phi) |\overline{\nabla}\theta|^2 \right] \mathrm{d}\overline{\Omega}. \tag{2.5}$$

The functions $g(\phi)$ and $h(\phi)$ are required to be monotonically increasing with the variable ϕ. The function $f(\phi)$ has a single minimum at $\phi = 1$ (for the application of grain boundary migration in solids). Equilibrium is characterized by a vanishing variational derivative and it is postulated according to the standard phase-field approach that relaxation is governed by rate equations of the following (dimensionless) form

$$Q\, \overline{\eta}_\phi\, \dot{\phi} = -\frac{\delta \overline{\mathcal{F}}_{\mathrm{KWC}}}{\delta \phi} = \overline{a}^2 \underline{\Delta}\phi - \frac{\partial f}{\partial \phi} - \overline{s}\, \frac{\partial g}{\partial \phi} |\overline{\nabla}\theta| - \frac{\overline{\varepsilon}^2}{2} \frac{\partial h}{\partial \phi} |\overline{\nabla}\theta|^2, \tag{2.6}$$

$$P\, \overline{\eta}_\theta\, \phi^2\, \dot{\theta} = -\frac{\delta \overline{\mathcal{F}}_{\mathrm{KWC}}}{\delta \theta} = \overline{\nabla} \cdot \left[\overline{\varepsilon}^2\, h(\phi)\, \overline{\nabla}\theta + \overline{s}\, g(\phi) \frac{\overline{\nabla}\theta}{|\overline{\nabla}\theta|} \right]. \tag{2.7}$$

In the above equations, Q and P are mobility functions which, in general, can depend on the state variables such that $Q = Q(\phi, \nabla\phi, \nabla\theta; T)$ and $P = P(\phi, \nabla\phi, \nabla\theta; T)$ with T being the temperature. The presence of the linear term $|\overline{\nabla}\theta|$ results in an infinite diffusion type of equation for the evolution of the field θ which requires some numerical regularization [Kobayashi and Giga, 1999]. Due to the coupling functions, both fields will have interfaces at the same locations but the width of the interface region will, in general, be smaller for θ than for ϕ [Lobkovsky and Warren, 2001].

3. Crystal Plasticity and Dislocation Densities

In this section, classic crystal plasticity theory is briefly introduced and, in particular, the link between the plasticity theory and dislocation densities is elaborated. Two types of dislocations were identified by Ashby [1970]: so-called statistically stored dislocations (SSDs) which are accumulated within grains during viscoplastic deformation due to random trapping and geometrically necessary dislocations GNDs, which are associated with incompatible deformations and can be expressed in terms of plastic strain gradients and lattice curvature.

3.1. *Kinematics of single crystal plasticity*

Let $\underline{\boldsymbol{X}}$ be the position of a material point in an undeformed body $\mathcal{B}_0$ and $\underline{\boldsymbol{x}}$ its position in the current, deformed state $\mathcal{B}_t$ and let the map $\underline{\boldsymbol{x}} = \underline{\boldsymbol{\varphi}}(\underline{\boldsymbol{X}}, t)$ describe the motion of material points between the reference and deformed configurations. The deformation gradient tensor $\underset{\sim}{\boldsymbol{F}} = \underline{\boldsymbol{\varphi}} \otimes \nabla_0$; $J = \det \underset{\sim}{\boldsymbol{F}} > 0$ is the material gradient of this map.

In plasticity, a multiplicative split $\underset{\sim}{\boldsymbol{F}} = \underset{\sim}{\boldsymbol{F}}^e \cdot \underset{\sim}{\boldsymbol{F}}^p$ is generally adopted [Kröner, 1959; Lee, 1969], whereby a fictitious, stress-free intermediate configuration is introduced. This intermediate configuration is not unique, as any rigid rotation of the body will result in another stress-free configuration. Some choice therefore has to be made to ensure the uniqueness of the multiplicative decomposition. In crystal plasticity, it is convenient to adopt an isoclinic intermediate configuration [Mandel, 1972, 1973] based on the observation that plastic deformation takes place by dislocation slip processes that leave the orientation of the lattice vectors intact compared to the reference state. This is demonstrated schematically in Fig. 2. There is thus a clear distinction between lattice directions on the one hand and material lines on the other, since lattice directions are not necessarily made up of the same points in the reference and deformed configurations and the glide of dislocations during plastic deformation does not distort the lattice, although it may shear material lines.

The evolution of plastic deformation by slip on N possible slip systems can be described in the intermediate configuration by

$$\dot{\underset{\sim}{\boldsymbol{F}}}^p \cdot \underset{\sim}{\boldsymbol{F}}^{p\,-1} = \sum_{\alpha=1}^{N} \dot{\gamma}^\alpha \underline{\boldsymbol{\ell}}^\alpha \otimes \underline{\boldsymbol{n}}^\alpha, \tag{3.1}$$

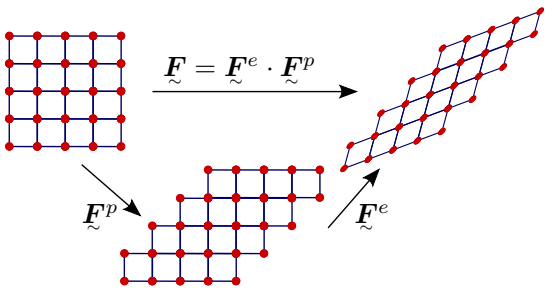

Fig. 2. In the isoclinic intermediate configuration, the lattice directors retain their orientation with respect to the undeformed configuration.

where $\underline{\boldsymbol{\ell}}^\alpha$ and $\underline{\boldsymbol{n}}^\alpha$ are the slip direction and slip plane normal and $\dot{\gamma}^\alpha$ is the slip rate which must be specified. Typically, for each load situation, $\dot{\gamma}^\alpha$ is non-zero only for a subset of preferred slip systems.

In this work, the coupled model is presented for small strains and small rotations (there is no distinction between referential and material configurations in the linearized theory). With $\underline{\boldsymbol{u}}$ being the displacement vector, the symmetric small strain tensor is given by $\underset{\sim}{\boldsymbol{\varepsilon}} = \mathrm{sym}(\underline{\boldsymbol{u}} \otimes \nabla) = \underset{\sim}{\boldsymbol{\varepsilon}}^e + \underset{\sim}{\boldsymbol{\varepsilon}}^p$ and $\underset{\sim}{\boldsymbol{\vartheta}} = \mathrm{skew}(\underline{\boldsymbol{u}} \otimes \nabla) = \underset{\sim}{\boldsymbol{\vartheta}}^e + \underset{\sim}{\boldsymbol{\vartheta}}^p$ is skew-symmetric and represents small rotations. The rate of the rotation $\underset{\sim}{\boldsymbol{\omega}} = \dot{\underset{\sim}{\boldsymbol{\vartheta}}}$ is the spin tensor. The linearized plastic rate of deformation and spin tensors are then given by

$$\dot{\underset{\sim}{\boldsymbol{\varepsilon}}}^p = \mathrm{sym}\left(\sum_{\alpha=1}^{N} \dot{\gamma}^\alpha \underline{\boldsymbol{\ell}}^\alpha \otimes \underline{\boldsymbol{n}}^\alpha\right), \tag{3.2}$$

$$\underset{\sim}{\boldsymbol{\omega}}^p = \dot{\underset{\sim}{\boldsymbol{\vartheta}}}^p = \mathrm{skew}\left(\sum_{\alpha=1}^{N} \dot{\gamma}^\alpha \underline{\boldsymbol{\ell}}^\alpha \otimes \underline{\boldsymbol{n}}^\alpha\right). \tag{3.3}$$

The elastic contributions follow from the additive decompositions, i.e., $\dot{\underset{\sim}{\boldsymbol{\varepsilon}}}^e = \dot{\underset{\sim}{\boldsymbol{\varepsilon}}} - \dot{\underset{\sim}{\boldsymbol{\varepsilon}}}^p$ and $\underset{\sim}{\boldsymbol{\omega}}^e = \dot{\underset{\sim}{\boldsymbol{\vartheta}}}^e = \underset{\sim}{\boldsymbol{\omega}} - \underset{\sim}{\boldsymbol{\omega}}^p$.

3.2. *Lattice curvature and the dislocation density tensor*

The elastic and plastic parts of $\underset{\sim}{\boldsymbol{F}}$ are, in general, not compatible (they are not the gradients of a vector field). A closed circuit C in $\mathcal{B}_0$ is therefore in general mapped onto an open circuit in the intermediate configuration by $\underset{\sim}{\boldsymbol{F}}^p$, and this is likewise true for the inverse mapping of a closed circuit c in $\mathcal{B}_t$ by $\underset{\sim}{\boldsymbol{F}}^{e-1}$. In the continuum description, the true Burgers vector for a smooth, oriented surface s in $\mathcal{B}_t$, with boundary c and containing $\mathrm{d}\underline{\boldsymbol{x}}$, can then be defined from the closure failure as

$$\underline{\boldsymbol{b}} = \int_c \underset{\sim}{\boldsymbol{F}}^{e-1} \cdot \mathrm{d}\underline{\boldsymbol{x}} = -\int_s [\nabla \times \underset{\sim}{\boldsymbol{F}}^{e-1}] \cdot \mathrm{d}\underline{\boldsymbol{s}} = \int_s \underset{\sim}{\boldsymbol{\alpha}} \cdot \mathrm{d}\underline{\boldsymbol{s}}, \tag{3.4}$$

where $\underline{\boldsymbol{n}}$ is the outward normal and $\underset{\sim}{\boldsymbol{\alpha}}$ is the dislocation density tensor which can thus be defined as

$$\underset{\sim}{\boldsymbol{\alpha}} \equiv -\nabla \times \underset{\sim}{\boldsymbol{F}}^{e-1} = -\frac{1}{J}[\nabla_0 \times \underset{\sim}{\boldsymbol{F}}^{p}] \cdot \underset{\sim}{\boldsymbol{F}}^{T}, \tag{3.5}$$

where the last equality can be found from push-back and pull-forward operations in (3.4). If the elastic stretches and rotations are small,[a] which can be expected for metals, the dislocation density tensor can be approximated as

$$\underset{\sim}{\boldsymbol{\alpha}} \approx \nabla \times \underset{\sim}{\boldsymbol{\vartheta}}^{e}. \tag{3.6}$$

For small deformations, the lattice curvature is given by the gradient of the pseudo-vector of the elastic rotation, i.e.,

$$\underset{\sim}{\boldsymbol{\kappa}} \equiv \overset{\times}{\underline{\boldsymbol{\vartheta}}}^{e} \otimes \nabla. \tag{3.7}$$

From Eqs. (3.6) and (3.7) follows the Nye relation [Nye, 1953]

$$\underset{\sim}{\boldsymbol{\alpha}} = \underset{\sim}{\boldsymbol{\kappa}}^{T} - \mathrm{tr}(\underset{\sim}{\boldsymbol{\kappa}})\underset{\sim}{\boldsymbol{I}}, \quad \underset{\sim}{\boldsymbol{\kappa}} = \underset{\sim}{\boldsymbol{\alpha}}^{\mathrm{T}} - \frac{1}{2}\mathrm{tr}(\underset{\sim}{\boldsymbol{\alpha}})\underset{\sim}{\boldsymbol{I}}. \tag{3.8}$$

GND development due to local deformation incompatibility results in size-dependent material behavior. Higher-order continuum crystal plasticity models which can take into consideration the effect of the dislocation density tensor are needed in this case, such as plastic strain gradient models [Fleck and Hutchinson, 1997] or Cosserat crystal plasticity [Forest *et al.*, 1997, 2001; Mayeur and McDowell, 2014]. The latter approach is used in this work and will be presented in the next section.

It appears that the lattice curvature tensor can be seen as an approximation of the full dislocation density tensor. Free energy potentials involving the norm and the square of the norm of the GND density tensor were considered by Forest and Guéninchault [2013], Wulfinghoff *et al.* [2015] in order to describe size effects in gradient crystal plasticity. They are closely related to the rank one and rank two lattice curvature potentials used in the KWC model. Relations between strain gradient, Cosserat and micromorphic crystal plasticity were established in Forest [2008], Cordero *et al.* [2012].

3.3. *Dislocations and work hardening*

As the dislocation density increases (both GND and SSD), additional plastic glide becomes more difficult and the material hardens. This can be taken into consideration by assuming that the critically resolved shear stress τ_c^{α} (the critical value of the stress projected on slip system α for which plasticity occurs) is proportional

[a]and in fact, if the elastic strain gradient also is small enough.

to the scalar dislocation density ρ according to Taylor [1934] and Franciosi *et al.* [1980]

$$\tau_c^\alpha = \mu b \sqrt{\sum_{\beta=1}^{N} h^{\alpha\beta}\rho^\beta}, \tag{3.9}$$

where N is the number of slip systems, μ is the shear modulus and b is the norm of the Burgers vector of the considered slip system family. The interaction matrix $h^{\alpha\beta}$ accounts for the anisotropic interaction between slip systems.

The evolution of dislocation content on slip system α can be described by competing mechanisms of multiplication and annihilation according to Kocks and Mecking [2003] and Teodosiu and Sidoroff [1976] as

$$\dot{\rho}^\alpha = \frac{1}{b}\left(\frac{1}{K}\sqrt{\sum_\beta \rho^\beta} - 2d\rho^\alpha\right)|\dot{\gamma}^\alpha|, \tag{3.10}$$

where the parameter K is a dislocation mobility constant and d is the critical annihilation distance between opposite sign dislocations.

Energy stored during viscoplastic deformation is also one of the most significant driving forces for grain boundary migration [Humphreys and Hatherly, 2004; Gottstein and Shvindlerman, 2010]. The stored energy and thereby driving pressure due to a dislocation density ρ can be expressed approximately as

$$\psi_\rho \approx \frac{1}{2}\mu b^2 \rho. \tag{3.11}$$

Gottstein and Shvindlerman [2010] gives typical values of the driving pressure due to stored dislocations that are several magnitudes larger than the driving pressures due to grain boundary energy.

4. The Coupled Cosserat Phase-Field Theory

This section is dedicated to an overview of the coupled Cosserat phase-field model proposed by Ask *et al.* [2018b] with some modifications that are detailed below. The model is valid for the case of small strains, small rotations and small curvatures. The model can be formulated within the large deformation framework, as proposed in Ask *et al.* [2018a].

4.1. *Kinematics, deformation measures and balance laws*

The Cosserat rotation tensor $\underset{\sim}{\mathfrak{R}}$ describes the rotation of a triad of directors attached to each material point from the initial to the deformed state. This rotation is, *a priori*, independent of the displacements so that six degrees of freedom are necessary to describe the motion of the material point: the displacement vector

$\underline{\boldsymbol{u}}$ and the microrotation pseudo-vector $\underline{\boldsymbol{\Theta}}$. In the small deformation setting, the Cosserat rotation tensor is then given by

$$\underset{\sim}{\mathfrak{R}} = \underset{\sim}{\boldsymbol{I}} - \underset{\sim}{\boldsymbol{\varepsilon}} \cdot \underline{\boldsymbol{\Theta}}, \tag{4.1}$$

and the linearized deformation measures are given by [Eringen and Kafadar, 1976; Forest *et al.*, 1997]

$$\underset{\sim}{\boldsymbol{e}} = \underline{\boldsymbol{u}} \otimes \nabla + \underset{\sim}{\boldsymbol{\varepsilon}} \cdot \underline{\boldsymbol{\Theta}}, \quad \underset{\sim}{\boldsymbol{\kappa}} = \underline{\boldsymbol{\Theta}} \otimes \nabla. \tag{4.2}$$

In the small strain setting, the decomposition of the deformation into elastic and plastic contributions is additive and given by

$$\underset{\sim}{\boldsymbol{e}} = \underset{\sim}{\boldsymbol{e}}^e + \underset{\sim}{\boldsymbol{e}}^p. \tag{4.3}$$

For simplicity, an elasto-plastic decomposition of the curvature tensor will not be pursued here, although it is possible following [Forest and Sievert, 2003]. Ask *et al.* [2018b] to introduce a third contribution in the decomposition of $\underset{\sim}{\boldsymbol{e}}$ in the form of a skew-symmetric eigendeformation with its own evolution equation. Here, a modified evolution law for the plastic deformation will be considered instead. The two approaches lead to formally identical governing equations.

By simple inspection, it is evident that the symmetric part of the Cosserat deformation is the usual small strain tensor, i.e.,

$$\mathrm{sym}(\underset{\sim}{\boldsymbol{e}}) = \underset{\sim}{\boldsymbol{\varepsilon}}, \tag{4.4}$$

whereas the skew-symmetric part is

$$\mathrm{skew}(\underset{\sim}{\boldsymbol{e}}) = \underset{\sim}{\boldsymbol{\vartheta}} + \underset{\sim}{\boldsymbol{\varepsilon}} \cdot \underline{\boldsymbol{\Theta}}. \tag{4.5}$$

Its rate can be written as

$$\dot{\underset{\sim}{\boldsymbol{e}}} = \dot{\underset{\sim}{\boldsymbol{\varepsilon}}} + \underset{\sim}{\boldsymbol{\omega}} + \underset{\sim}{\boldsymbol{\varepsilon}} \cdot \dot{\underline{\boldsymbol{\Theta}}}, \tag{4.6}$$

with the skew-symmetric part represented by a pseudo-vector

$$\dot{\overset{\times}{\underline{\boldsymbol{e}}}} = \overset{\times}{\underline{\boldsymbol{\omega}}} - \dot{\underline{\boldsymbol{\Theta}}}. \tag{4.7}$$

This latter expression relates the relative rotation of the material and the motion of the microstructural directors that is described by the Cosserat rotation. In particular, taking into account plasticity and introducing the elastic and plastic spin pseudo-vectors $\overset{\times}{\underline{\boldsymbol{\omega}}}{}^p := \dot{\overset{\times}{\underline{\boldsymbol{e}}}}{}^p$ and $\overset{\times}{\underline{\boldsymbol{\omega}}}{}^e := \overset{\times}{\underline{\boldsymbol{\omega}}} - \overset{\times}{\underline{\boldsymbol{\omega}}}{}^p$, respectively, the rate of the skew-symmetric deformation can be expressed as

$$\overset{\times}{\underline{\boldsymbol{\omega}}}{}^e - \dot{\underline{\boldsymbol{\Theta}}} = \dot{\overset{\times}{\underline{\boldsymbol{e}}}}{}^e. \tag{4.8}$$

The above expression provides a link between the lattice and microrotation rates that enables a formulation, where the Cosserat directors remain parallel to the

lattice vectors as the body deforms. This is achieved by enforcement of the internal constraint

$$\overset{\times}{\underset{\sim}{\boldsymbol{e}}}^{e} \equiv 0. \tag{4.9}$$

either on the constitutive level [Forest *et al.*, 1997, 2000; Mayeur *et al.*, 2011; Mayeur and McDowell, 2014; Blesgen, 2014] or directly using Lagrange multipliers.

Finally, in order to account for migrating grain boundaries, the Cosserat theory is enhanced with a phase-field variable $\phi \in [0, 1]$ which is interpreted in this context as a coarse-grained measure of crystalline order. In the bulk of an undeformed grain, the order parameter takes the value $\phi = 1$, whereas $\phi < 1$ in grain boundaries or even inside plastically deformed grains due to build-up of SSD.

The balance equations and corresponding boundary conditions for the coupled formulation are found by applying the method of virtual power on the set of virtual field variables

$$\mathcal{V} = \{\dot{\phi}, \nabla\dot{\phi}, \dot{\underline{\boldsymbol{u}}}, \dot{\underline{\boldsymbol{u}}} \otimes \nabla, \dot{\underline{\boldsymbol{\Theta}}}, \dot{\underline{\boldsymbol{\Theta}}} \otimes \nabla\}, \tag{4.10}$$

and their associated generalized stresses [Ask *et al.*, 2018b; Abrivard *et al.*, 2012a; Ammar *et al.*, 2009a]. By adopting the formalism of Gurtin [1996], Gurtin and Lusk [1999] for the phase-field, the integration of the phase-field equations in the overall approach is straightforward. The resulting field and boundary equations are given by

$$\nabla \cdot \underline{\boldsymbol{\xi}}_{\phi} + \pi_{\phi} + \pi_{\phi}^{\text{ext}} = 0 \quad \text{in } \Omega, \tag{4.11}$$

$$\underset{\sim}{\boldsymbol{\sigma}} \cdot \nabla + \underline{\boldsymbol{f}}^{\text{ext}} = \underline{\mathbf{0}} \quad \text{in } \Omega, \tag{4.12}$$

$$\underset{\sim}{\boldsymbol{m}} \cdot \nabla + 2\,\overset{\times}{\underline{\boldsymbol{\sigma}}} + \underline{\boldsymbol{c}}^{\text{ext}} = \underline{\mathbf{0}} \quad \text{in } \Omega, \tag{4.13}$$

$$\underline{\boldsymbol{\xi}}_{\phi} \cdot \underline{\boldsymbol{n}} = \pi_{\phi}^{c} \quad \text{on } \partial\Omega, \tag{4.14}$$

$$\underset{\sim}{\boldsymbol{\sigma}} \cdot \underline{\boldsymbol{n}} = \underline{\boldsymbol{f}}^{c} \quad \text{on } \partial\Omega, \tag{4.15}$$

$$\underset{\sim}{\boldsymbol{m}} \cdot \underline{\boldsymbol{n}} = \underline{\boldsymbol{c}}^{c} \quad \text{on } \partial\Omega. \tag{4.16}$$

The stress $\underset{\sim}{\boldsymbol{\sigma}}$ associated with the Cosserat deformation $\underset{\sim}{\boldsymbol{e}}$ is not the usual Cauchy stress and contains a skew-symmetric contribution that also appears in the balance equation for the couple-stress $\underset{\sim}{\boldsymbol{m}}$ which is work conjugate to the curvature/wryness tensor $\underset{\sim}{\boldsymbol{\kappa}}$. The microstresses π_{ϕ} and $\underline{\boldsymbol{\xi}}_{\phi}$ in (4.11) are associated with the phase-field ϕ and its gradient $\nabla\phi$, respectively. External body forces and couples are denoted by superscript $\langle\bullet\rangle^{\text{ext}}$ and contact forces and couples by superscript $\langle\bullet\rangle^{c}$, with $\underline{\boldsymbol{n}}$ the outward normal to the boundary $\partial\Omega$ of the body Ω.

4.2. *Constitutive and evolution equations*

The general constitutive equations used in this work comply with the thermodynamic principles [Ask *et al.*, 2018b]. In order to recover the phase-field dynamics,

it is assumed that the stress π_ϕ contains energetic and dissipative contributions so that

$$\pi_\phi = \pi_\phi^{\mathrm{eq}} + \pi_\phi^{\mathrm{neq}}. \tag{4.17}$$

The following expressions are proposed for the energetic quantities

$$\pi_\phi^{\mathrm{eq}} = -\frac{\partial \psi}{\partial \phi}, \tag{4.18}$$

$$\underline{\boldsymbol{\xi}}_\phi = \frac{\partial \psi}{\partial \nabla \phi}, \tag{4.19}$$

$$\underset{\sim}{\boldsymbol{\sigma}} = \frac{\partial \psi}{\partial \underset{\sim}{\boldsymbol{e}}^e}, \tag{4.20}$$

$$\underset{\sim}{\boldsymbol{m}} = \frac{\partial \psi}{\partial \underset{\sim}{\boldsymbol{\kappa}}}, \tag{4.21}$$

assuming that

$$\rho\Psi = \psi(\phi, \nabla\phi, \underset{\sim}{\boldsymbol{e}}^e, \underset{\sim}{\boldsymbol{\kappa}}, r^\alpha), \tag{4.22}$$

where Ψ is the Helmholtz energy density and r^α are internal variables related to the inelastic behavior. For the dissipative processes, it is assumed that there exists a dissipation potential

$$\Omega = \Omega^p(\underset{\sim}{\boldsymbol{\sigma}}) + \Omega^\alpha(R^\alpha) + \Omega^\phi(\pi_\phi^{\mathrm{neq}}), \tag{4.23}$$

where

$$R^\alpha = \frac{\partial \psi}{\partial r^\alpha} \tag{4.24}$$

are thermodynamic forces associated with r^α and evolution equations, including the flow and hardening rules, are derived from the dissipation potential

$$\dot{\underset{\sim}{\boldsymbol{e}}}^p = \frac{\partial \Omega^p}{\partial \underset{\sim}{\boldsymbol{\sigma}}}, \quad \dot{r}^\alpha = -\frac{\partial \Omega^\alpha}{\partial R^\alpha}, \quad \dot{\phi} = -\frac{\partial \Omega^\phi}{\partial \pi_\phi^{\mathrm{neq}}}. \tag{4.25}$$

The potential Ω chosen in the following fulfils convexity conditions which ensure positive dissipation. The formulation presented here differs somewhat from the one presented in Ask *et al.* [2018b] in that there are fewer contributions to the dissipation potential. This is for two reasons. First, a dissipative contribution to the stress $\underset{\sim}{\boldsymbol{\sigma}}$ was considered in the previous work which led to a separate evolution law for the relative rotation in the spirit of the KWC model. This contribution is necessary in the KWC model but superfluous in the coupled approach and therefore not considered here. Second, the separate eigendeformation-type tensor introduced in Ask *et al.* [2018b] is considered as a part of the plastic deformation in this work and its evolution is derived from Ω^p.

4.3. *Coupled model*

The free energy density for the coupled problem is given by Ask *et al.* [2018b]

$$\psi(\phi, \nabla\phi, \underset{\sim}{\boldsymbol{e}}^e, \underset{\sim}{\boldsymbol{\kappa}}, r^\alpha) = f_0 \left[f(\phi) + \frac{a^2}{2}|\nabla\phi|^2 + sg(\phi)\|\underset{\sim}{\boldsymbol{\kappa}}\| + \frac{\varepsilon^2}{2} h(\phi)\|\underset{\sim}{\boldsymbol{\kappa}}\|^2 \right] + \frac{1}{2}\underset{\sim}{\boldsymbol{\varepsilon}}^e : \underset{\approx}{\boldsymbol{E}}^s : \underset{\sim}{\boldsymbol{\varepsilon}}^e + 2\mu_c \, \underline{\boldsymbol{e}}^{\times e} \cdot \underline{\boldsymbol{e}}^{\times e} + \psi_\rho(\phi, r^\alpha). \tag{4.26}$$

The first line can be considered a generalization to three dimensions of the KWC energy (2.5). It contains a grain boundary term due to the phase-field ϕ and a contribution due to the lattice curvature tensor $\underset{\sim}{\boldsymbol{\kappa}}$. The coupling functions $g(\phi)$ and $h(\phi)$ are required to be non-negative and to increase monotonously with ϕ. The parameter f_0 has dimension [Pa] and a, s and ε have dimension [m]. While the main motivation for including the linear term corresponding to $\|\nabla\underset{\sim}{\boldsymbol{\kappa}}\|$ in the KWC model was to localize the grain boundaries, the relationship between the lattice curvature and the GND density tensor allows for a physical interpretation, where the linear term represents the self energy of the GNDs and the quadratic term is an interaction energy [Ohno and Okumura, 2007; Mesarovic *et al.*, 2015; Wulfinghoff *et al.*, 2015]. The link between the KWC model and a higher-order crystal plasticity theory was also recognized in the work of Admal *et al.* [2018], who formulated a similar coupled approach using the full GND density tensor. A consequence of including the linear term is that the energy density (4.26) becomes non-differentiable at zero curvature and in the numerical treatment, it is therefore replaced by a regularized quantity [Kobayashi and Giga, 1999; Abrivard *et al.*, 2012a; Wulfinghoff *et al.*, 2015; Admal *et al.*, 2018; Ask *et al.*, 2018b] to avoid the singularity at $\|\underset{\sim}{\boldsymbol{\kappa}}\| = 0$.

The second line in (4.26) contains the energy contribution due to symmetric and skew-symmetric elastic deformation. A standard quadratic form is adopted for the symmetric strain with the (possibly anisotropic) elasticity tensor $\underset{\approx}{\boldsymbol{E}}^s$. By choosing the Cosserat parameter μ_c to be large enough, the skew-symmetric part of the deformation is penalized and the Cosserat microrotation is required to follow the lattice orientation, thus approaching the constraint (4.9). The following state laws are obtained

$$\mathrm{sym}(\underset{\sim}{\boldsymbol{\sigma}}) = \underset{\approx}{\boldsymbol{E}}^s : \underset{\sim}{\boldsymbol{\varepsilon}}, \tag{4.27}$$

$$\underline{\boldsymbol{\sigma}}^{\times} = 2\mu_c \underline{\boldsymbol{e}}^{\times e}, \tag{4.28}$$

$$\underset{\sim}{\boldsymbol{m}} = f_0 \left[sg(\phi)\frac{1}{\|\underset{\sim}{\boldsymbol{\kappa}}\|} + \varepsilon^2 \, h(\phi) \right] \underset{\sim}{\boldsymbol{\kappa}}, \tag{4.29}$$

$$\pi_\phi^{\mathrm{eq}} = -f_0 \left[1 - \phi - s\,\frac{\partial g}{\partial \phi}\|\underset{\sim}{\boldsymbol{\kappa}}\| - \frac{\varepsilon^2}{2}\frac{\partial h}{\partial \phi}\|\underset{\sim}{\boldsymbol{\kappa}}\|^2 \right] - \sum_{\alpha=1}^{N} \frac{1}{2}\mu r^{\alpha 2}, \tag{4.30}$$

$$\underline{\boldsymbol{\xi}}_\phi = f_0 \, a^2 \nabla\phi. \tag{4.31}$$

The very last term in (4.26) is the stored energy due to accumulated dislocations. It is taken to be

$$\psi_\rho(\phi, r^\alpha) = \phi \sum_{\alpha=1}^{N} \frac{1}{2} \mu r^{\alpha 2}, \tag{4.32}$$

where N is the number of slip systems and r^α are internal variables. Note that there is a coupling with the phase-field variable ϕ. This coupling ensures that the stored energy acts as a driving force for grain boundary migration. The internal variables are assumed to be related to the scalar dislocation densities via

$$r^\alpha = b \sqrt{\sum_{\beta=1}^{N} h^{\alpha\beta} \rho^\beta}. \tag{4.33}$$

This leads to the following Taylor hardening expression

$$R^\alpha = \frac{\partial \psi}{\partial r^\alpha} = \phi \mu \, r^\alpha = \phi \mu \, b \sqrt{\sum_{\beta=1}^{N} h^{\alpha\beta} \rho^\beta}. \tag{4.34}$$

For the thermodynamic force R^α which is now interpreted as the critical resolved shear stress on slip system α.

The plastic dissipation potential Ω^p is assumed to be given by

$$\Omega^p = \sum_{\alpha=1}^{N} \frac{K_v}{n+1} \left\langle \frac{|\tau^\alpha| - R^\alpha}{K_v} \right\rangle^{n+1} + \frac{1}{2} \eta_\star^{-1}(\phi, \nabla\phi, \underset{\sim}{\boldsymbol{\kappa}}) \overset{\times}{\underline{\boldsymbol{\sigma}}} \cdot \overset{\times}{\underline{\boldsymbol{\sigma}}}, \tag{4.35}$$

where $\langle \bullet \rangle = \mathrm{Max}(\bullet, 0)$ and τ^α is the resolved shear stress on slip system α that can be calculated as

$$\tau^\alpha = \underline{\boldsymbol{\ell}}^\alpha \cdot \underset{\sim}{\boldsymbol{\sigma}} \cdot \underline{\boldsymbol{n}}^\alpha, \tag{4.36}$$

where $\underline{\boldsymbol{\ell}}^\alpha$ and $\underline{\boldsymbol{n}}^\alpha$ are, respectively, the slip direction and normal to the slip plane. Note that the stress tensor is not symmetric so that a contribution to the resolved shear stress arises from the double contraction of the skew–symmetric stress with the skew–symmetric part of the tensor $\underline{\boldsymbol{\ell}}^\alpha \otimes \underline{\boldsymbol{n}}^\alpha$. This contribution can be interpreted as a size-dependent kinematic hardening, as shown in Sedláček and Forest [2000], Sedláček *et al.* [2002], Forest and Sedláček [2003] and Forest [2008]. The second term in (4.35) is supposed to be active only in the grain boundary regions which can be achieved by constructing $\eta_\star(\phi, \nabla\phi, \underset{\sim}{\boldsymbol{\kappa}})$ in terms of its arguments so that it is small inside the grain boundaries and large inside the grains. The pseudo-vector $\overset{\times}{\underline{\boldsymbol{\sigma}}}$ contains the skew-symmetric contributions to the stress. The evolution of plastic deformation follows from (4.25) and (4.35)

$$\dot{\underset{\sim}{\boldsymbol{e}}}^p = \sum_{\alpha=1}^{N} \dot{\gamma}^\alpha \, \underline{\boldsymbol{\ell}}^\alpha \otimes \underline{\boldsymbol{n}}^\alpha + \eta_\star^{-1}(\phi, \nabla\phi, \underset{\sim}{\boldsymbol{\kappa}}) \, \mathrm{skew}(\underset{\sim}{\boldsymbol{\sigma}}), \tag{4.37}$$

with the slip rate given by

$$\dot{\gamma}^\alpha = \left\langle \frac{|\tau^\alpha| - R^\alpha}{K_v} \right\rangle^n \operatorname{sign} \tau^\alpha, \tag{4.38}$$

whereas the first part of (4.37) is a classic crystal flow rule, the second part is included to take into account the reorientation which takes place in the interface region during grain boundary migration as a result of atomic reshuffling processes. It is a purely skew-symmetric contribution, i.e., it acts only on the plastic spin. Specifically, the skew-symmetric plastic deformation can be written as

$$\overset{\times}{\underline{\boldsymbol{e}}}{}^p = \overset{\times}{\underline{\boldsymbol{e}}}{}^{\text{slip}} + \overset{\times}{\underline{\boldsymbol{e}}}{}^\star, \tag{4.39}$$

with

$$\dot{\overset{\times}{\underline{\boldsymbol{e}}}}{}^{\text{slip}} = \overset{\times}{\underline{\boldsymbol{\omega}}}{}^p - \overset{\times}{\underline{\boldsymbol{\omega}}}{}^\star, \quad \underset{\sim}{\boldsymbol{\omega}}{}^p - \underset{\sim}{\boldsymbol{\omega}}{}^\star = \operatorname{skew}\left(\sum_{\alpha=1}^{N} \dot{\gamma}^\alpha \, \underline{\boldsymbol{\ell}}^\alpha \otimes \underline{\boldsymbol{n}}^\alpha \right), \tag{4.40}$$

$$\dot{\overset{\times}{\underline{\boldsymbol{e}}}}{}^\star = \overset{\times}{\underline{\boldsymbol{\omega}}}{}^\star, \quad \overset{\times}{\underline{\boldsymbol{\omega}}}{}^\star = \eta_\star^{-1}(\phi, \nabla\phi, \underset{\sim}{\boldsymbol{\kappa}}) \overset{\times}{\underline{\boldsymbol{\sigma}}}. \tag{4.41}$$

The quantity $\overset{\times}{\underline{\boldsymbol{e}}}{}^\star$ which is here associated with the plastic spin was introduced in the form of an eigendeformation with an associated evolution law in Ask *et al.* [2018b]. In order to compare the two formulations, consider the elastic skew-symmetric deformation, which is given by

$$\overset{\times}{\underline{\boldsymbol{e}}}{}^e = \overset{\times}{\underline{\boldsymbol{\vartheta}}}{}^e - \underline{\boldsymbol{\Theta}} = \overset{\times}{\underline{\boldsymbol{\vartheta}}} - \overset{\times}{\underline{\boldsymbol{e}}}{}^p - \underline{\boldsymbol{\Theta}} = \overset{\times}{\underline{\boldsymbol{\vartheta}}} - \overset{\times}{\underline{\boldsymbol{e}}}{}^{\text{slip}} - \overset{\times}{\underline{\boldsymbol{e}}}{}^\star - \underline{\boldsymbol{\Theta}}. \tag{4.42}$$

When the Cosserat microrotations are taken to represent the lattice orientation measured relative to a fixed frame, they are in general non-zero in the reference configuration. If the deformations are zero, it must hold that $\overset{\times}{\underline{\boldsymbol{\vartheta}}}(t=0) = \underline{\boldsymbol{0}}$. In Ask *et al.* [2018b], this was resolved by adopting the following initial conditions

$$\overset{\times}{\underline{\boldsymbol{e}}}{}^\star(t=0) = -\underline{\boldsymbol{\Theta}}(t=0). \tag{4.43}$$

The same assumption can be made in this case, however unlike in Ask *et al.* [2018b], this will also have, as a consequence that

$$\overset{\times}{\underline{\boldsymbol{e}}}{}^p(t=0) = -\underline{\boldsymbol{\Theta}}(t=0), \tag{4.44}$$

since here the skew-symmetric plastic deformation does not only contain the contribution due to plastic slip. Non-zero initial conditions on the plastic deformation were also adopted in Admal *et al.* [2018] in order to accommodate a polycrystal made of differently oriented grains.

From (4.42), it is clear that an evolution of the Cosserat microrotation due to a migrating grain boundary would result in a non-zero $\overset{\times}{\underline{\boldsymbol{e}}}{}^e$ and thereby a skew-symmetric stress in the region swept by the moving front. Due to (4.41), this stress is relaxed by evolution of $\overset{\times}{\underline{\boldsymbol{e}}}{}^\star$.

The evolution of the scalar dislocation densities ρ^α is assumed to follow a modified Kocks-Mecking Teodosiu evolution law [Abrivard *et al.*, 2012a,b; Ask *et al.*, 2018b] such that

$$\dot{\rho}^\alpha = \begin{cases} \dfrac{1}{b}\left(\dfrac{1}{K}\sqrt{\displaystyle\sum_\beta \rho^\beta} - 2d\rho^\alpha\right)|\dot{\gamma}^\alpha| - \rho^\alpha\, C_D\, A(|\underset{\sim}{\boldsymbol{\kappa}}|)\dot{\phi} & \text{if } \dot{\phi} > 0 \\ \dfrac{1}{b}\left(\dfrac{1}{K}\sqrt{\displaystyle\sum_\beta \rho^\beta} - 2d\rho^\alpha\right)|\dot{\gamma}^\alpha| & \text{if } \dot{\phi} \leq 0. \end{cases} \tag{4.45}$$

The additional term compared to (3.10) accounts for static recovery due to dislocations being annihilated in the wake of a migrating grain boundary. Full recovery is obtained for sufficiently high values of the parameter C_D. The function $A(|\underset{\sim}{\boldsymbol{\kappa}}|)$ is chosen so that it localizes the static recovery process to the grain boundary regions.

The evolution of the phase-field ϕ is chosen to be governed by a quadratic dissipation potential [Gurtin, 1996; Abrivard *et al.*, 2012a]

$$\Omega^\phi = \frac{1}{2}\eta_\phi^{-1}(\phi, \nabla\phi, {}^\sharp\underset{\sim}{\boldsymbol{\Gamma}}^e)\pi_\phi^{\text{neq}2}, \tag{4.46}$$

so that

$$\eta_\phi(\phi, \nabla\phi, {}^\sharp\underset{\sim}{\boldsymbol{\Gamma}}^e)\dot{\phi} = -\pi_\phi^{\text{neq}}. \tag{4.47}$$

5. Numerical Solution of the Triple Junction Problem

The model presented in the previous section has been implemented for numerical simulations by finite elements in the Z-set code [Z-set package, 2013]. Details on the numerical implementation can be found in Ammar *et al.* [2009a] and Ask *et al.* [2018b]. Since the implementation is in two dimensions, rotation only takes place around one axis (in this case the z-axis) and the Cosserat pseudo-vector of microrotations only has one non-zero contribution θ such that $\underline{\boldsymbol{\Theta}} = [0\ 0\ \theta]^T$. Figure 3 shows the geometry of the triple junction problem. Dirichlet conditions are assumed for ϕ, θ and the displacements $\underline{\boldsymbol{u}}$, with $u_x = u_y = 0$ along the boundaries. The computational domain is assumed to be $10 \times 10\,\mu\text{m}^2$ and is discretized by 50×50 quadratic elements with reduced integration. The simulations are performed on a non-dimensionalized system according to Ask *et al.* [2018b], with $\overline{x} = x/\Lambda$ and $\overline{y} = y/\Lambda$, where $\Lambda = 1\,\mu\text{m}$. The term $\eta_\star(\phi, \nabla\phi, \underset{\sim}{\boldsymbol{\kappa}})$ in (4.41) is taken to be

$$\eta_\star(\nabla\theta) = \hat{\eta}_\star\left[1 - \left[1 - \frac{\mu_p}{\varepsilon}\right]\exp(-\beta_P\,\varepsilon|\nabla\theta|)\right], \tag{5.1}$$

with the coefficients chosen such that $\mu_p/\varepsilon = 1000$ and $\beta_P\,\varepsilon = 1000$.

The model parameters are given in Table 1. Values that are reasonable for pure copper have been chosen, although a formal fit to experimental data has not been carried out. Dimensionless time $\overline{t} = t/\tau_0$ is used in the simulations. A

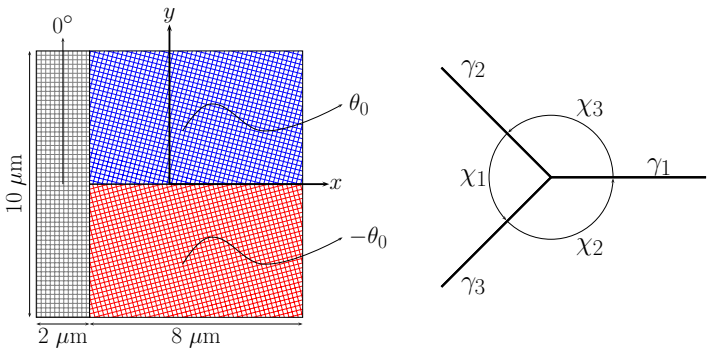

Fig. 3. Geometry and initial conditions for the triple junction problem (left) and definition of angles and grain boundaries for the Herring's equation (right).

Table 1. Model parameters.

	f_0	a	s	ε	η_ϕ	$\hat{\eta}_\star$	μ	λ	μ_c
Unit	[MPa]	[μm]	[μm]	[μm]	[MPa s]	[MPa s]	[GPa]	[GPa]	[GPa]
Value	1.8	0.3	2.	2.	0.1 $f_0\,\tau_0$	0.1 $f_0\,\tau_0$	46.1	69.2	1.8

physical timescale can be set by choosing the parameter τ_0. Initial conditions must be provided for ϕ, θ and the viscoplastic pseudo-vector $\overset{\times}{\underline{\boldsymbol{e}}}^\star$. The initial fields $\phi(\overline{t}=0)$ and $\theta(\overline{t}=0)$ are constructed by means of sinh and tanh functions, respectively, whereas $\overset{\times}{\underline{\boldsymbol{e}}}^\star$ is initialized so that $\overset{\times}{\underline{\boldsymbol{e}}}^e(\overline{t}=0)=\underline{\mathbf{0}}$.

The linear term $\|\underset{\sim}{\boldsymbol{\kappa}}\|$ in the energy density (4.26) is regularized according to the same scheme proposed by Warren *et al.* [2003] that was used in Ask *et al.* [2018b], where $\|\underset{\sim}{\boldsymbol{\kappa}}\|$ is replaced by the function $A_c(\|\underset{\sim}{\boldsymbol{\kappa}}\|)$ with

$$A_c(\xi)=\begin{cases}\dfrac{c}{2}\,\xi^2 & \text{for } 0\le\xi\le 1/c,\\[2ex] \xi-\dfrac{1}{2c} & \text{for } \xi>1/c,\end{cases} \tag{5.2}$$

where c is a large and positive constant (in the simulations $c=10^4$ is used).

5.1. *Equilibrium of the triple junction*

In two dimensions, the triple junction problem concerns finding the equilibrium solution when three grains have a common intersection. The solution will be of the format shown schematically in Fig. 3 (right). If the grain boundary energies γ_i are known, the Herring equation [Herring, 1951] can be used to calculate the corresponding angles of the intersection according to

$$\frac{\gamma_1}{\sin(\chi_1)}=\frac{\gamma_2}{\sin(\chi_2)}=\frac{\gamma_3}{\sin(\chi_3)}. \tag{5.3}$$

Note that only for equal grain boundary energies (which would be the case for equal misorientation between all grains), the angles χ_i are equal and each 120°. Here, an initial geometry according to Fig. 3 will be used, with the left-hand side grain having an initial orientation of 0° and the other two grains $\pm\theta_0$. This will result in two identical angles $\chi_2 = \chi_3$ and some manipulation of Eq. (5.3) results in

$$\cos(\chi_2) = -\frac{1}{2}\frac{\gamma_1}{\gamma_2}, \tag{5.4}$$

with $\chi_1 = 360° - 2\,\chi_2$.

The corresponding grain boundary energies for the chosen misorientations θ_0 can be calculated using the results of asymptotic expansion of the orientation phase-field model by Lobkovsky and Warren [2001]. The derivation of the asymptotic solution is rather long and will not be repeated here, the reader is referred to Ask *et al.* [2018b] for more details. Due to the strongly coupled nature of the two fields ϕ and θ in the model, the solution in the sharp interface limit must be resolved numerically. The calculated *dimensionless* grain boundary energies $\overline{\gamma}_1$ and $\overline{\gamma}_2$ for $\theta_0 = \pm 7.5°$ and $\theta_0 = \pm 5°$ are given in Table 2, together with the corresponding angle χ_2 calculated from (5.4).

Figure 4 shows the equilibrium solutions for $\theta_0 = \pm 5°$ (left) and $\theta_0 = \pm 7.5°$ (right). It is evident from the figure that different misorientations result in different angles χ_i, as expected. Due to the diffuse nature of the interfaces and the discrete

Table 2. Solution to the Herring equilibrium and numerical (FE) results.

$\pm\theta_0$	$\overline{\gamma}_1$	$\overline{\gamma}_2$	χ_2	$\overline{x}_{\mathrm{TP}}$	χ_2 (FE)
5°	0.115	0.071	144°	4 ± 0.1	$144.5° \pm 0.3°$
7.5°	0.138	0.096	136°	2 ± 0.1	$135° \pm 0.6°$

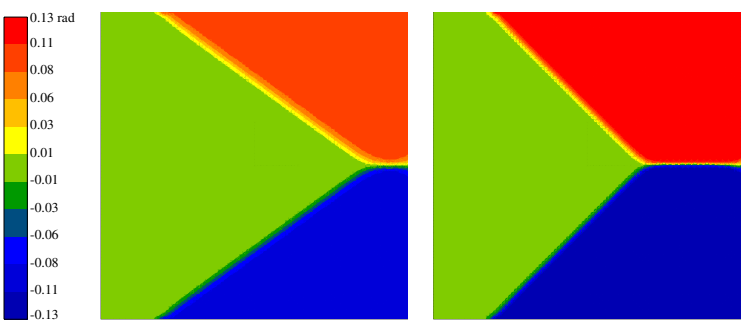

Fig. 4. The equilibrium solution with $\theta_0 = \pm 5°$ (left) and $\theta_0 = \pm 7.5°$ (right). It is evident from the images that the angles of the triple junction are different for the different grain misorientations. Due to the diffuse nature of the interfaces and the discrete finite element mesh, the exact point of the triple junction and thereby the angles can only be measured approximately. For $\theta_0 = \pm 5°$, the triple junction is at approximately $\overline{x} = 4 \pm 0.1$ and for $\theta_0 = \pm 7.5°$, it is at approximately $\overline{x} = 2 \pm 0.1$ (origin is at the center of the computational domain).

finite element mesh, the exact point of the triple junction and thereby the angles can only be measured approximately. For $\theta_0 = \pm 5^\circ$, the triple junction is at approximately $\overline{x}_{\mathrm{TP}} = 4$ and for $\theta_0 = \pm 7.5^\circ$, it is at approximately $\overline{x}_{\mathrm{TP}} = 2$ (the origin is at the center of the computational domain). With the initial geometry given by Fig. 3, and recalling that Dirichlet boundary conditions are used, the angle χ_2 found in the simulations can then be calculated as

$$\chi_2 \approx \arctan((\overline{x}_{\mathrm{TP}} + 3)/5) + \pi/2. \tag{5.5}$$

The resulting approximate values for χ_2 are presented in Table 2. The agreement is very good between the (semi-)analytic results and the simulations.

5.2. *Parameter study and grain boundary mobility*

In the proposed coupled model, there is no separate relaxational dynamics for θ. Instead, local reorientation in the grain boundary to allow for migration is made possible by the evolution law for the plastic deformation and specifically the plastic spin term $\underset{\sim}{\boldsymbol{\omega}}^\star$. Ideally, the mobility of the grain boundary should be determined only by the phase-field relaxational (mobility) parameter η_ϕ. However, if the relaxation of the plastic spin is too slow, this will slow down or prevent the grain boundary from migrating.

Simulations were carried out with $\hat{\eta}_\star$ varying by several orders of magnitude in order to study its impact on the grain boundary migration. The other model parameters are those in Table 1. For the angles, $\theta_0 = \pm 7.5^\circ$ was used. Note that the absolute value of $\hat{\eta}_\star$ is of less interest than the ratio $r_\eta = \hat{\eta}_\star/\eta_\phi$. Measuring the exact position of the triple junction during the simulations is not practical, instead the profile of the phase-field ϕ along $\overline{y} = 0$ is traced over time for different values of r_η. The triple junction is approximately positioned where the gradient of the phase-field is maximum. In Fig. 5 (top), the profile of ϕ along $\overline{y} = 0$ at $\overline{t} = 10$ is shown for $r_\eta = 1000, 100, 10, 1$ and 0.1, respectively. For all $r_\eta \leq 10$, the same profile is recovered. Figure 5 (bottom) shows the profile of ϕ along $\overline{y} = 0$ at $\overline{t} = 1, 10$ and 50 for $r_\eta = 100$ (red lines) $r_\eta = 10$ (black lines) and $r_\eta = 1$ (blue lines). Again, there is not much difference between $r_\eta = 10$ and $r_\eta = 1$. This gives an indication that, provided $\hat{\eta}_\star$ is chosen sufficiently small with respect to η_ϕ, this parameter does not influence the grain boundary mobility. Similar results were found by Ask *et al.* [2018b], however in that work there was an additional relaxational equation for the Cosserat orientation which is not included here. This feature makes the model simpler for practical use compared to the original KWC formulation.

5.3. *Stresses in the grain boundary*

Figure 6 shows the evolution of the triple junction over time, from left to right $\overline{t} = 0.1, 1, 10$ and 50. The phase-field ϕ is shown in the top row and the orientation θ in the bottom row. A misorientation of $\theta_0 = \pm 7.5^\circ$ was used together with the

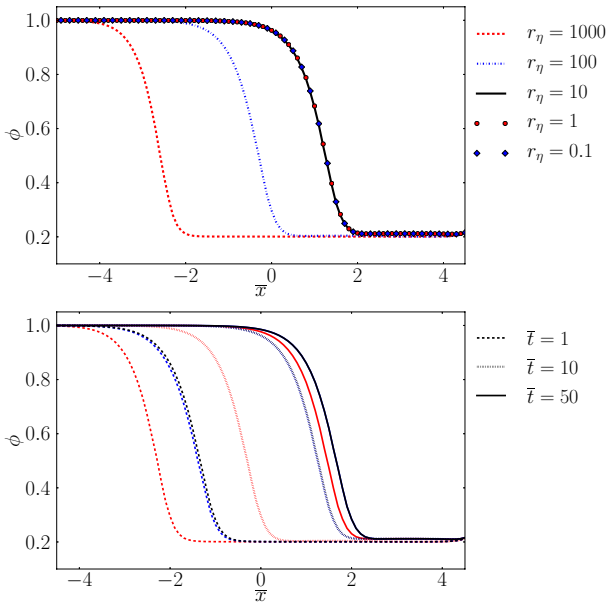

Fig. 5. The influence of the parameter $\hat{\eta}_\star$ on the mobility of the grain boundaries. The top figure shows the profile of the phase-field ϕ along $\overline{y} = 0$ at $\overline{t} = 10$ for different ratios $r_\eta = \hat{\eta}_\star/\eta_\phi$. The triple junction is approximately positioned, where the gradient of the phase-field is maximum. The bottom figure shows the profile of ϕ along $\overline{y} = 0$ at $\overline{t} = 1, 10$ and 50 for $r_\eta = 100$ (red lines) $r_\eta = 10$ (black lines) and $r_\eta = 1$ (blue lines). For $\overline{t} = 10$ and 50 black and blue lines overlap (Color online).

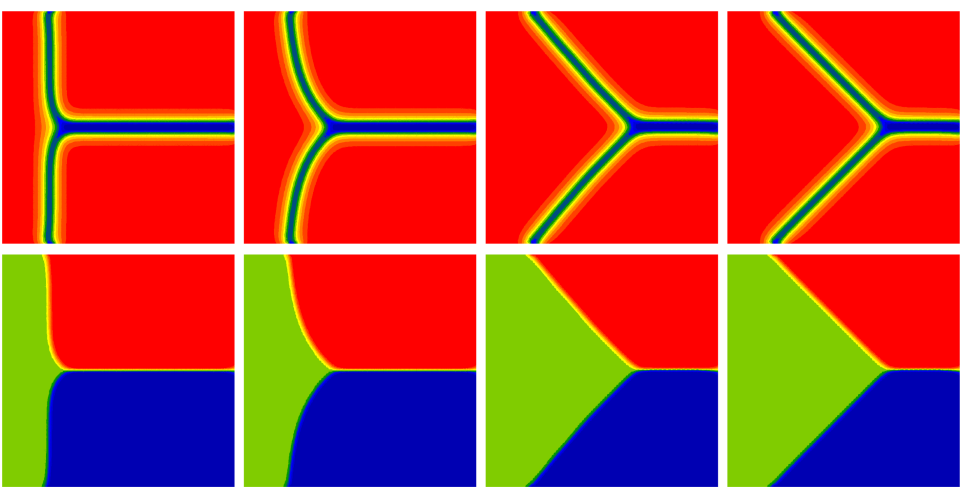

Fig. 6. Evolution of the triple junction over time, from left to right $\overline{t} = 0.1, 1, 10$ and 50. The top plots show $\phi \in [0, 1]$ and the bottom plots show $\theta \in [-7.5°, 7.5°]$.

material parameters in Table 1. It appears that the correct angles χ_i are stabilized first and then the triple point migrates to minimize the grain boundary curvature.

The grain boundary migration is not expected to give rise to any significant strains in the simulations for the triple junction problem. However, there are still stresses present. The microstress π_ϕ which belongs to the phase-field ϕ and is given by Eq. (4.30) is non-zero in the grain boundary region. The dissipative part of this stress drives the evolution of ϕ according to (4.47). The progress of the microstress π_ϕ over time is shown in Fig. 7 and the progress of the components of the generalized stress $\underline{\boldsymbol{\xi}}_\phi$ are shown in Fig. 8. The microstresses are governed by the balance Eq. (4.11). Taking into consideration (4.11) and (4.47) together with the additive

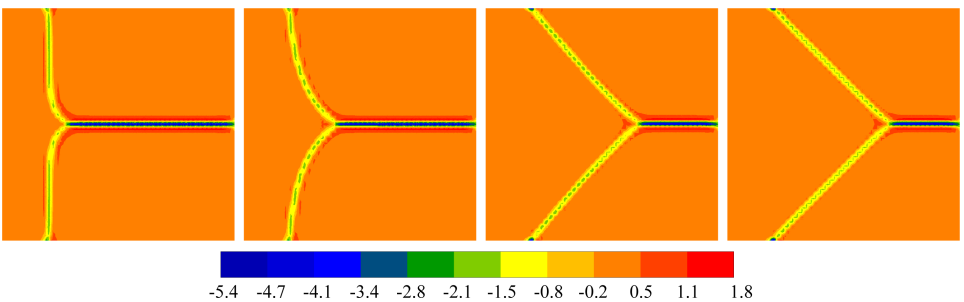

Fig. 7. Microstress $\pi_\phi \in [-5.4, 1.8]$ MPa at time $\overline{t} = 0.1, 1, 10$ and 50 (left to right). Note that as the solution stabilizes, the dissipative part π_ϕ^{neq} goes to zero and only the energetic contribution remains.

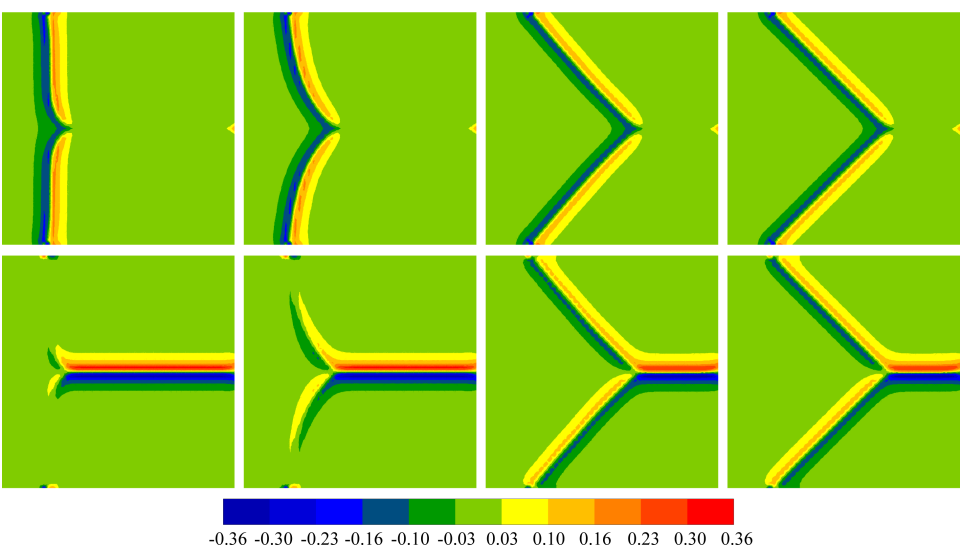

Fig. 8. Microstress $\underline{\boldsymbol{\xi}}_\phi \in [-0.36, 0.36]$ MPa at time $\overline{t} = 0.1, 1, 10$ and 50 (left to right). The top row shows the x-component and the bottom row shows the y-component.

decomposition (4.17) of π_ϕ, the evolution of the phase-field ϕ is given by

$$\eta_\phi \dot{\phi} = -\pi_\eta^{\text{neq}} = \nabla \cdot \underline{\boldsymbol{\xi}}_\eta + \pi_\phi^{\text{eq}}. \tag{5.6}$$

Both capillary forces (grain boundary curvature) and stored energy drive the evolution of the phase-field. Equation (5.6) highlights the competing contributions from interface and bulk terms, associated, respectively, with $\nabla\phi$ via $\underline{\boldsymbol{\xi}}_\phi$ on the one hand and ϕ and the associated microstresses π_ϕ on the other hand. The couple-stress $\underset{\sim}{\boldsymbol{m}}$ is governed by (4.13). Due to the coupling between terms in ϕ and terms in $\|\underset{\sim}{\boldsymbol{\kappa}}\|$ in the energy density (4.26), the couple-stress $\underset{\sim}{\boldsymbol{m}}$ contains mixed contributions. In the orientation phase-field inspired model, this coupling is what ensures that the orientation evolves along with ϕ (and vice versa). However, in the original KWC model, only gradients of orientation entered the energy function, not the orientation itself. The energy could therefore always be lowered by rotating adjacent grains toward a smaller misorientation. In the present model, this bulk rotation is prevented by the Cosserat coupling term which ensures that, in the bulk, the Cosserat directors remain parallel to the lattice vectors.

When the grain boundaries migrate and the orientation changes, the skew-symmetric stress $\overset{\times}{\underline{\boldsymbol{\sigma}}}$ becomes non-zero. This, in turn, drives the evolution of $\underset{\sim}{\boldsymbol{\omega}}^\star$ which relaxes the skew-symmetric stress and allows for the grain boundary to migrate. In the two-dimensional simulations, there is only one non-zero contribution $\overset{\times}{\sigma} = \overset{\times}{\sigma}_z$ to $\overset{\times}{\underline{\boldsymbol{\sigma}}}$. The rate at which the skew-symmetric stress vanishes depends on the parameter $\hat{\eta}_\star$. If this viscosity-type parameter is large relative to the parameter η_ϕ which controls the grain boundary mobility, the stress does not have time to relax and it remains, slowing down the grain boundary migration as evidenced by the fact that a larger ratio $r_\eta = \hat{\eta}_\star/\eta_\phi$ implies a slower evolution towards equilibrium. The effect of the parameter $\hat{\eta}_\star$ is demonstrated in Fig. 9 which shows the skew-symmetric stress contribution $\overset{\times}{\sigma}$ at $\overline{t} = 0.1$ for three different values of $r_\eta = \hat{\eta}_\star/\eta_\phi$. In particular, for $r_\eta = 1$, the skew-symmetric stress has already relaxed after $\overline{t} = 0.1$.

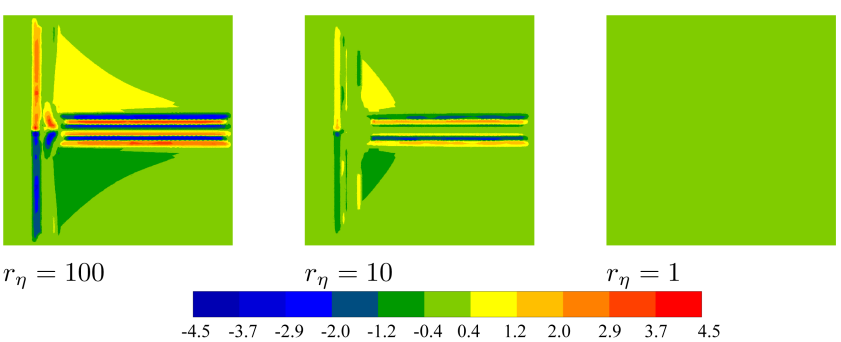

Fig. 9. Skew-symmetric stress contribution $\overset{\times}{\sigma}$ (in MPa) at $\overline{t} = 0.1$ for three different values of $r_\eta = \hat{\eta}_\star/\eta_\phi$. From left to right, top to bottom: $r_\eta = 100$, 10 and 1.

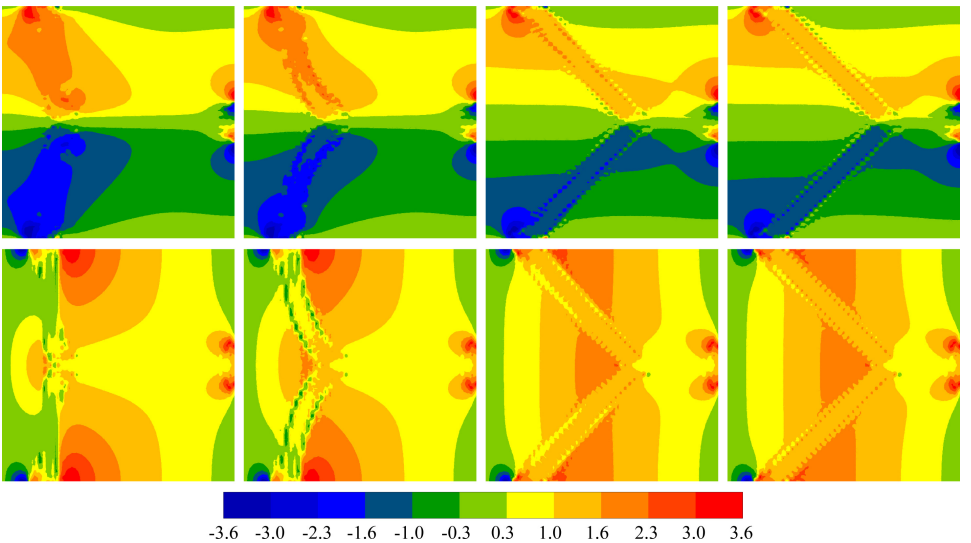

Fig. 10. The non-zero contributions to the couple-stress $\underset{\sim}{\boldsymbol{m}} \in [-3.6, 3.6]$ MPa at time $\overline{t} = 0.1, 1, 10$ and 50 (left to right). The top row shows the x-component (m_{zx}) and the bottom row shows the y-component (m_{zy}).

By construction, the choice of the viscosity type parameter $\hat{\eta}_\star$ influences the relaxation time for the skew-symmetric stress in the grain boundaries. It is demonstrated that this in turn plays a role for the grain boundary migration which is slowed down if the skew-symmetric stress does not relax sufficiently fast.

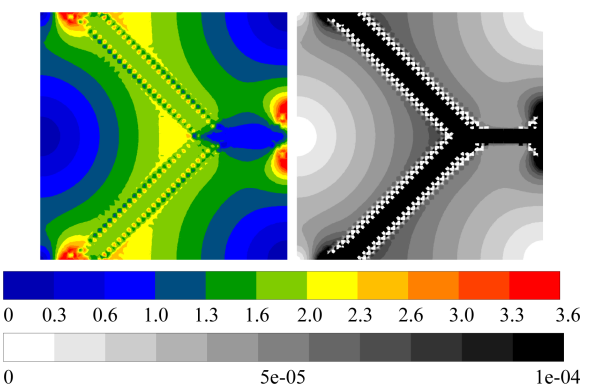

Fig. 11. The norm of the couple-stress $\underset{\sim}{\boldsymbol{m}}$ (in MPa) and and the norm of the curvature tensor $\|\underset{\sim}{\boldsymbol{\kappa}}\|$ (right) at time $\overline{t} = 50$ (left). The scale for normalized $\|\underset{\sim}{\boldsymbol{\kappa}}\|$ has been set so that the maximum value is 10^{-4} corresponding to the cutoff in the numerical regularization. There is some irregularity in the cutoff region which may be in part due to the interpolation from the integration points of the finite elements to the nodes but also to actual noise in the solution.

The components of the couple-stress tensor $\underset{\sim}{\boldsymbol{m}}$ (the only non-zero components are m_{zx} and m_{zy} which are referred to as the x- and y-components, respectively) are given in Fig. 10. The divergence of $\underset{\sim}{\boldsymbol{m}}$ vanishes with vanishing skew-symmetric stress according to (4.13). Unlike $\underline{\boldsymbol{\xi}}_{\phi}$, the couple-stress $\underset{\sim}{\boldsymbol{m}}$ is not localized to the grain boundary regions. Due to the Dirichlet conditions, there are some boundary effects, but more importantly, there is a separation between the solution in the boundary and in the bulk. This can be explained by the numerical regularization (5.2). Figure 11 shows the norm of $\underset{\sim}{\boldsymbol{m}}$ next to $\|\underset{\sim}{\boldsymbol{\kappa}}\|$, where the scale has been adjusted so that the normalized $\|\underset{\sim}{\boldsymbol{\kappa}}\| \geq 10^{-4}$ (the cutoff for the regularization) is shown in black.

6. Summary and Outlook

The coupling of phase-field and mechanical models for the simulation of grain boundary migration under load still is a largely open theoretical question. The most popular MPF approach does not properly account for the role of the development of lattice curvature inside the grains in recrystallization processes. In the present work, the full coupling is performed within the Cosserat mechanical framework thus extending the KWC approach. A slightly modified version of the coupled crystal plasticity phase-field model proposed in Ask *et al.* [2018b] was presented. By a short review of the underlying theory, the motivation for using an orientation phase-field model together with the Cosserat crystal plasticity theory was elaborated. The coupling between the orientation phase-field model and the Cosserat theory is very natural, as they both contain orientation as a degree of freedom. The model has earlier been demonstrated to have the ability to predict grain boundary migration due to both grain boundary energy and stored energy gradients due to scalar dislocation densities. In this work, it was demonstrated that the model correctly predicts the equilibrium solution to the well-known triple junction problem. It was also demonstrated how the material parameters may influence the grain boundary migration and for which choices of material parameters skew-symmetric stresses in the grain boundary vanish or remain and counteract grain boundary mobility, respectively. The current implementation of the model can be used to simulate grain boundary migration in two-dimensional polycrystals. Three-dimensional simulations remain challenging due to the need for a fine discretization of the mobile interface regions and the numerical complexity of the coupled model. In addition, the interpretation of the diffuse orientation across a boundary region in three dimensions requires some attention.

The coupling of a higher-order crystal plasticity theory and an orientation phase-field model was also successfully pursued by Admal *et al.* [2018]. In the proposed model by Admal *et al.* [2018], the grain boundary migration is always associated with plastic slip in the region swept by the grain boundary. Grain boundary migration may take place due to grain boundary curvature (due to the phase-field contribution) or in the form of shear-induced grain boundary migration. Stored

energy is not included as a driving force but could be added in a similar fashion as in the present work. The model proposed in the present work accounts for grain boundary migration due to capillary forces (grain boundary curvature) or stored dislocation densities. Shear-induced grain boundary migration is not considered. The lattice orientation may change due to plastic slip processes but grain boundary migration is not associated with slip processes in the interface region.

In the Cosserat crystal plasticity, the GND density tensor is approximated by the curvature tensor, whereas the strain gradient plasticity model uses the full GND density tensor which is more exact. On the other hand, the model by Admal *et al.* [2018] considers the plastic slips of each slip system as degrees of freedom, each of them associated with a balance equation. This is in contrast with the present work which considers only three additional degrees of freedom (the components of the Cosserat orientation vector) for any number of slip systems. This is true also for the corresponding large deformation theory [Ask *et al.*, 2018a].

Although the formulations presented in this work and in Admal *et al.* [2018] are not identical and have been applied to slightly different problems of coupled deformation and grain boundary migration, it is clear that this type of modeling framework is promising and represents a major step toward a truly unified theory applicable to microstructure evolution during deformation and recrystallization processes.

The finite deformation theory of the model is the subject of the work [Ask *et al.*, 2018a]. Its corresponding numerical implementation is a challenging task which will make possible the simulation of processes such as cold rolling involving very large plastic strains and lattice rotation and curvature. The main numerical challenges regarding the model itself stems from the strong coupling and the singular diffusive type equation resulting from the particular energy density of the orientation phase field model. In addition, there are challenges related to the need for high resolution at interface regions which may be solved by incorporating adaptive meshing techniques. It should also be noted that although the model is presented for isothermal conditions in this work (for brevity), temperature effects remain to be incorporated at various suitable places in the model.

Acknowledgments

This Project has received funding from the European Research Council (ERC) Under the European Union's Horizon 2020 research and innovation program (Grant Agreement No. 707392 MIGRATE).

References

Abrivard, G., Busso, E. P., Forest, S. and Appolaire, B. [2012a] "Phase field modeling of grain boundary motion driven by curvature and stored energy gradients. Part I: Theory and numerical implementation," *Philosophical Magazine* **92**, 3618–3642.

Abrivard, G., Busso, E. P., Forest, S. and Appolaire, B. [2012b] "Phase field modeling of grain boundary motion driven by curvature and stored energy gradients. Part II: Application to recrystallisation," *Philosophical Magazine* **92**, 3643–3664.

Admal, N. C., Po, G. and Marian, J. [2018] "A unified framework for polycrystal plasticity with grain boundary evolution," *International Journal of Plasticity*, doi: https://doi.org/10.1016/j.ijplas.2018.01.014, http://www.sciencedirect.com/science/article/pii/S0749641917305557.

Allen, S. M. and Cahn, J. W. [1979] "A microscopic theory for antiphase boundary motion and its application to antiphase domain coarsening," *Acta Metallurgica* **27**(6), 1085–1095.

Ammar, K., Appolaire, B., Cailletaud, G., Feyel, F. and Forest, S. [2009a] "Finite element formulation of a phase field model based on the concept of generalized stresses," *Computational Materials Science* **45**, 800–805.

Ammar, K., Appolaire, B., Cailletaud, G. and Forest, S. [2009b] "Combining phase field approach and homogenization methods for modeling phase transformation in elasto-plastic media," *European Journal of Computational Mechanics* **18**(5–6), 485–523.

Ammar, K., Appolaire, B., Cailletaud, G. and Forest, S. [2011] "Phase field modeling of elasto-plastic deformation induced by diffusion controlled growth of a misfitting spherical precipitate," *Philosophical Magazine Letters* **91**(3), 164–172.

Ashby, M. [1970] "The deformation of plastically non–homogeneous materials," *Philosophical Magazine* **21**, 399–424.

Ask, A., Forest, S., Appolaire, B. and Ammar, K. [2018a] "A Cosserat–phase-field theory of crystal plasticity and grain boundary migration at finite deformation", *Continuum Mechanics and Thermodynamics*, doi:https://doi.org/10.1007/s00161-018-0727-6.

Ask, A., Forest, S., Appolaire, B., Ammar, K. and Salman, O. U. [2018b] "A cosserat crystal plasticity and phase field theory for grain boundary migration," *Journal of the Mechanics and Physics of Solids* **115**, 167–194, doi:https://doi.org/10.1016/j.jmps.2018.03.006.

Bernacki, M., Resk, H., Coupez, T. and Logé, R. E. [2009] "Finite element model of primary recrystallization in polycrystalline aggregates using a level set framework," *Modeling and Simulation in Materials Science and Engineering* **17**, 064006.

Blesgen, T. [2014] "Deformation patterning in three-dimensional large-strain Cosserat plasticity," *Mechanics Research Communications* **62**, 37–43.

Blesgen, T. [2017] "A variational model for dynamic recrystallization based on Cosserat plasticity," *Composites Part B*: *Engineering* **115**, 236–243.

Cermelli, P. and Gurtin, M. E. [2001] "On the characterization of geometrically necessary dislocations in finite plasticity," *Journal of the Mechanics and Physics of Solids* **49**(7), 1539–1568.

Chen, L., Chen, J., Lebensohn, R. A., Ji, Y. Z., Heo, T. W., Bhattacharyya, S., Chang, K., Mathaudhu, S., Liu, Z. K. and Chen, L. Q. [2015] "An integrated fast fourier transform-based phase-field and crystal plasticity approach to model recrystallization of three dimensional polycrystals," *Computer Methods in Applied Mechanics and Engineering* **285**, 829–848.

Cordero, N. M., Forest, S., Busso, E. P., Berbenni, S. and Cherkaoui, M. [2012] "Grain size effects on plastic strain and dislocation density tensor fields in metal polycrystals," *Computational Materials Science* **52**, 7–13.

Cosserat, E. and Cosserat, F. [1909] *Théorie des corps déformables* (Hermann, Paris).

de Rancourt, V., Ammar, K., Appolaire, B. and Forest, S. [2016] "Homogenization of viscoplastic constitutive laws within a phase field approach," *Journal of the Mechanics and Physics of Solids* **88**, 291–319, doi:https://doi.org/10.1016/j.jmps.2015.12.026.

Eringen, A. C. and Kafadar, C. B. [1976] "Part 1. Polar Field Theories," in *Continuum Physics*, ed. A. C. Eringen, Vol. 4 (Academic Press), pp. 1–73.

Fleck, N. and Hutchinson, J. [1997] "Strain gradient plasticity," *Adv. Appl. Mech.* **33**, 295–361.

Forest, S. [2008] "Some links between Cosserat, strain gradient crystal plasticity and the statistical theory of dislocations," *Philosophical Magazine* **88**, 3549–3563.

Forest, S., Barbe, F. and Cailletaud, G. [2000] "Cosserat modeling of size effects in the mechanical behaviour of polycrystals and multiphase materials," *International Journal of Solids and Structures* **37**, 7105–7126.

Forest, S., Boubidi, P. and Sievert, R. [2001] "Strain localization patterns at a crack tip in generalized single crystal plasticity," *Scripta Materialia* **44**, 953–958.

Forest, S., Cailletaud, G. and Sievert, R. [1997] "A Cosserat theory for elastoviscoplastic single crystals at finite deformation," *Archives of Mechanics* **49**(4), 705–736.

Forest, S. and Guéninchault, N. [2013] "Inspection of free energy functions in gradient crystal plasticity," *Acta Mechanica Sinica* **29**, 763–772.

Forest, S. and Sedláček, R. [2003] "Plastic slip distribution in two–phase laminate microstructures: Dislocation–based versus generalized–continuum approaches," *Philosophical Magazine A* **83**, 245–276.

Forest, S. and Sievert, R. [2003] "Elastoviscoplastic constitutive frameworks for generalized continua," *Acta Mechanica* **160**, 71–111.

Franciosi, P., Berveiller, M. and Zaoui, A. [1980] "Latent hardening in copper and aluminium single crystals," *Acta Metallurgica* **28**(3), 273–283.

Gottstein, G. and Shvindlerman, L. [2010] *Grain Boundary Migration in Metals* (CRC Press, Berlin).

Gurtin, M. E. [1996] "Generalized Ginzburg-Landau and Cahn-Hilliard equations based on a microforce balance," *Physica D*: *Nonlinear Phenomena* **92**(3), 178–192.

Gurtin, M. E. [2002] "A gradient theory of single-crystal viscoplasticity that accounts for geometrically necessary dislocations," *Journal of the Mechanics and Physics of Solids* **50**(1), 5–32.

Gurtin, M. E. and Lusk, M. T. [1999] "Sharp-interface and phase-field theories of recrystallization in the plane," *Physica D*: *Nonlinear Phenomena* **130**(1–2), 133–154.

Güvenç, O., Bambach, M. and Hirt, G. [2014] "Coupling of crystal plasticity finite element and phase field methods for the prediction of SRX kinetics after hot working," *Steel Research International* **85**(6), 999–1009.

Güvenç, O., Henke, T., Laschet, G., Böttger, B., Apel, M., Bambach, M. and Hirt, G. [2013] "Modeling of static recrystallization kinetics by coupling crystal plasticity FEM and multiphase field calculations," *Computer Methods in Materials Science* **13**(2), 368–374.

Hallberg, H. [2011] "Approaches to modeling of recrystallization," *Metals* **1**(1), 16–48.

Hektor, J., Ristinmaa, M., Hallberg, H., Hall, S. A. and Iyengar, S. [2016] "Coupled diffusion-deformation multiphase field model for elastoplastic materials applied to the growth of cu6sn5," *Acta Materialia* **108**, 98–109.

Herring, C. [1951] "Some theorems on the free energies of crystal surfaces," *Physical Review* **82**, 87–93.

Humphreys, F. and Hatherly, M. [2004] *Recrystallization and Related Annealing Phenomena* (Elsevier).

Kobayashi, R. and Giga, Y. [1999] "Equations with singular diffusivity," *Journal of Statistical Physics* **95**(5–6), 1189–1220.

Kobayashi, R., Warren, J. A. and Carter, W. C. [2000] "A continuum model of grain boundaries," *Physica D* **140**(1–2), 141–150.

Kocks, U. F. and Mecking, H. [2003] "Physics and phenomenology of strain hardening: The FCC case," *Progress in Materials Science* **48**, 171–273.

Kröner, E. [1959] "Allgemeine Kontinuumstheorie der Versetzungen und Eigenspannungen," *Archive for Rational Mechanics and Analysis* **4**, 273–334.

Lee, E. H. [1969] "Elastic-plastic deformation at finite strains," *Journal of Applied Mechanics* **36**, 1–6.

Lobkovsky, A. E. and Warren, J. A. [2001] "Sharp interface limit of a phase-field model of crystal grains," *Physical Review E* **63**(5), 051605.

Mandel, J. [1972] *Plasticité classique et viscoplasticité*, CISM Courses and Lectures No. 97, Udine, 1971 (Springer-Verlag).

Mandel, J. [1973] "Equations constitutives et directeurs dans les milieux plastiques et viscoplastiques," *Int. J. Solids Structures* **9**, 725–740.

Mayeur, J. and McDowell, D. [2014] "A comparison of gurtin type and micropolar theories of generalized single crystal plasticity," *International Journal of Plasticity* **57**, 29–51, doi:http://dx.doi.org/10.1016/j.ijplas.2014.01.010.

Mayeur, J., McDowell, D. and Bammann, D. [2011] "Dislocation–based micropolar single crystal plasticity: Comparison of multi — and single criterion theories," *Journal of the Mechanics and Physics of Solids* **59**, 398–422.

Mesarovic, S. D., Forest, S. and Jaric, J. P. [2015] "Size-dependent energy in crystal plasticity and continuum dislocation models," *Proc. R. Soc. A*: *Math. Phys. Eng. Sci.* **471**(2175), 20140868, 19 p.

Nye, J. [1953] "Some geometrical relations in dislocated crystals," *Acta Metall.* **1**, 153–162.

Ohno, N. and Okumura, D. [2007] "Higher–order stress and grain size effects due to self–energy of geometrically necessary dislocations," *Journal of the Mechanics and Physics of Solids* **55**, 1879–1898.

Rollett, A. [1997] "Overview of modeling and simulation of recrystallization," *Progress in Materials Science* **42**(1), 79–99.

Sedláček, R., Blum, W., Kratochvil, J. and Forest, S. [2002] "Subgrain formation during deformation: Physical origin and consequences," *Metallurgical and Materials Transactions* **33A**, 319–327.

Sedláček, R. and Forest, S. [2000] "Non-local plasticity at microscale: A dislocation-based model and a Cosserat model," *Physica Status Solidi* (*b*) **221**, 583–596.

Steinbach, I. [2009] "Phase-field models in materials science," *Modeling and Simulation in Materials Science and Engineering* **17**(7), 073001.

Steinbach, I. and Pezzolla, F. [1999] "A generalized field method for multiphase transformations using interface fields," *Physica D*: *Nonlinear Phenomena* **134**(4), 385–393.

Steinbach, I., Pezzolla, F., Nestler, B., Seeßelberg, M., Prieler, R., Schmitz, G. J. and Rezende, J. L. L. [1996] "A phase field concept for multiphase systems," *Physica D*: *Nonlinear Phenomena* **94**(3), 135–147.

Takaki, T., Hisakuni, Y., Hirouchi, T., Yamanaka, A. and Tomita, Y. [2009] "Multi-phase-field simulations for dynamic recrystallization," *Computational Materials Science* **45**(4), 881–888.

Takaki, T. and Tomita, Y. [2010] "Static recrystallization simulations starting from predicted deformation microstructure by coupling multi-phase-field method and finite element method based on crystal plasticity," *International Journal of Mechanical Sciences* **52**(2), 320–328.

Takaki, T., Yamanaka, A., Higa, Y. and Tomita, Y. [2007] "Phase-field model during static recrystallization based on crystal-plasticity theory," *Journal of Computer-Aided Materials Design* **14**(1), 75–84.

Takaki, T., Yoshimoto, C., Yamanaka, A. and Tomita, Y. [2014] "Multiscale modeling of hot-working with dynamic recrystallization by coupling microstructure evolution and macroscopic mechanical behavior," *International Journal of Plasticity* **52**, 105–116, doi:https://doi.org/10.1016/j.ijplas.2013.09.001.

Taylor, G. I. [1934] "The mechanism of plastic deformation of crystals. Part I — theoretical," *Proceedings of the Royal Society of London A*: *Mathematical*, *Physical and Engineering Sciences* **145**(855), 362–387.

Teodosiu, C. and Sidoroff, F. [1976] "A theory of finite elastoviscoplasticity of single crystals," *International Journal of Engineering Science* **14**, 165–176.

Vondrous, A., Bienger, P., Schreijäg, S., Selzer, M., Schneider, D., Nestler, B., Helm, D. and Mönig, R. [2015] "Combined crystal plasticity and phase-field method for recrystallization in a process chain of sheet metal production," *Computational Mechanics* **55**(2), 439–452.

Warren, J. A., Kobayashi, R., Lobkovsky, A. E. and Carter, W. C. [2003] "Extending phase field models of solidification to polycrystalline materials," *Acta Materialia* **51**(20), 6035–6058.

Wulfinghoff, S., Forest, S. and Böhlke, T. [2015] "Strain gradient plasticity modeling of the cyclic behavior of laminate microstructures," *Journal of the Mechanics and Physics of Solids* **79**, 1–20, doi:10.1016/j.jmps.2015.02.008.

Z-set package [2013] "Non-linear material & structure analysis suite, www.zset-software.com,".

Zhao, P., Low, T. S. E., Wang, Y. and Niezgoda, S. R. [2016] "An integrated full-field model of concurrent plastic deformation and microstructure evolution: Application to 3d simulation of dynamic recrystallization in polycrystalline copper," *International Journal of Plasticity* **80**, 38–55, doi:https://doi.org/10.1016/j.ijplas.2015.12.010.